RESOLUTION OF FLUID-STRUCTURE COUPLED PROBLEMS WITH FLOW USING THE BOUNDARY ELEMENT METHOD

Robin Le Mestre, Jean-Sébastien Schotté, Olivier Doaré

RESOLUTION OF FLUID-STRUCTURE COUPLED PROBLEMS WITH FLOW USING THE BOUNDARY ELEMENT METHOD

Robin Le Mestre
ONERA, Châtillon, France; ENSTA Paris, IPP, IMSIA, EDF, CEA, CNRS, Palaiseau, France

Jean-Sébastien Schotté
ONERA, Châtillon, France

Olivier Doaré
ENSTA Paris, IPP, IMSIA, EDF, CEA, CNRS, Palaiseau, France

ABSTRACT

Effects of fluid-structure coupling on the dynamic behaviour of flexible airship can be modelled with a potential, incompressible, inviscid flow. A new formalism to study linear variations of the flow induced on the fluid-structure interface in a time dependent ambient flow is introduced. The features of the Boundary Element Method used to solve this problem numerically are exhibited. Numerical results of the linear model are compared with analytical and non linear numerical results, assessing the validity and the limitations of the approach.

1. INTRODUCTION

Fluid-structure dynamical interaction of deformable bodies with potential flows have various applications, from bubbles (Galper (1995) - Riccardi et al (2020)) and airships (Li et al, 2009) to submerged pipes (Veron et al, 2016). In the case of airships, fluid-structure interaction solutions have been found, for instance by (Liu et al, 2009) in the case of quasi steady incompressible viscous flow by coupling CFD and FEM codes for the fluid and structure respectively on a hull-fin configuration. However this coupling of a flowing fluid with a vibrating structure at high Reynolds number remains a challenge to solve at the scale of airships using CFD methods. A potential flow approach was proposed (Li et al, 2009) by deriving the inviscid, incompressible and irrotational linear variations of the fluid loads applied on a flexible airship. In their model, the hull is simplified as a cantilever beam from both fluid and structure point of view, using an Eulerian specification of the fluid and solving the Lagrange equations of the coupled system. In this study, the linear variations of the potential, inviscid, irrotational flow induced by the airship three dimensional hull are modelled by linearization of the associated integral representation with an Arbitrary Lagrangian Eulerian specification. The problem is solved numerically using a Boundary Element Method (BEM), offering both low computational cost, in comparison with Finite Element or other methods, and high fidelity of the solution at the interface. The method enables to solve fluid-structure interaction problems with strong coupling effects (due to the similar orders of magnitude of the fluid and structure densities) and highly flexible structures.

Section 2 of this paper introduces the equations governing the velocity of the fluid and the associated hypothesis as well as a linearized integral representation of the potential flow solution. Section 3 will focus on the numerical implementation of the BEM and its validation with analytical cases. The ability of the linear model to capture the physics of the fluid will be discussed with a comparison to non linear results. Section 4 proposes a conclusion on the performance of this method and perspectives regarding the future extensions of the model.

2. MODEL

2.1. Governing equations

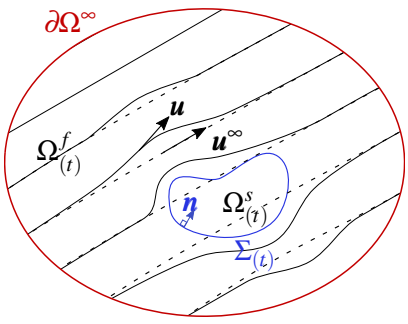

Figure 1. Scheme of the fluid and solid domain.

We consider a structure deforming in an inviscid flow. The effects of the turbulent boundary layer are neglected. The fluid evolves in a domain $\Omega^f_{(t)}$ bounded

by the fluid-structure interface $\Sigma_{(t)}$ and its exterior boundary $\partial\Omega^{\infty}$. We consider the case where no circulation is induced in the flow $\boldsymbol{u}$, enabling to express it with a potential ϕ defined up to a spatial constant by:

$$\boldsymbol{u} = \boldsymbol{\nabla}\phi \quad \text{in } \Omega^{f}_{(t)}. \tag{1}$$

The ambient flow is defined as the flow in the absence of structure (dashed streamlines of figure 1):

$$\boldsymbol{u}^{\infty}_{(\boldsymbol{x},t)} = \boldsymbol{\nabla}\phi^{\infty}_{(\boldsymbol{x},t)} \quad \text{in } \Omega^{\infty}, \tag{2}$$

supposed to be time variant and inhomogeneous. For a potential flow, the incompressibility condition writes:

$$\Delta\phi^{\infty} = 0 \quad \text{in } \Omega^{\infty}. \tag{3}$$

When a moving structure is introduced, the domain Ω^{∞} is divided into a fluid and a solid sub-domains $\Omega^{f}_{(t)}$ and $\Omega^{s}_{(t)}$ separated by the fluid-structure interface $\Sigma_{(t)}$. The flow $\boldsymbol{u}$ (continuous streamlines of figure 1) in the fluid domain is decomposed into an ambient flow $\boldsymbol{u}^{\infty}$ and a potential perturbed flow $\boldsymbol{u}^{p} = \boldsymbol{\nabla}\phi^{p}$ such that:

$$\boldsymbol{u} = \boldsymbol{\nabla}\phi^{\infty} + \boldsymbol{\nabla}\phi^{p} \quad \text{in } \Omega^{f}_{(t)}. \tag{4}$$

The flow incompressibility combined with (3) and (4) provides

$$\boxed{\Delta\phi^{p} = 0 \quad \text{in } \Omega^{f}_{(t)}.} \tag{5}$$

One can show with energetic considerations that the perturbations of the fluid decrease rapidly to infinity:

$$\boxed{\boldsymbol{\nabla}\phi^{p} = o\left(r^{-\frac{3}{2}}\right) \quad \text{on } \partial\Omega^{\infty}.} \tag{6}$$

The inviscid kinematic boundary condition is introduced as

$$\boldsymbol{u}.\boldsymbol{n} = \frac{\partial\boldsymbol{\xi}}{\partial t}.\boldsymbol{n} \quad \text{on } \Sigma_{(t)}, \tag{7}$$

$\boldsymbol{n}$ being the interface normal, oriented outward the fluid (see figure 1). Equation (7) is valid when both Reynolds and Stokes numbers (ratio between inertia and viscosity effects of the fluid) are small:

$$\begin{aligned} Re &= \frac{\rho_f U^{\infty} L}{\mu} \gg 1 \\ St &= \frac{\rho_f \Omega L^2}{\mu} \gg 1, \end{aligned} \tag{8}$$

where L and Ω are characteristic length and pulsation of the structure, ρ_f and μ are the density and the viscosity of the fluid respectively, and U^{∞} is a characteristic velocity of the ambient flow. When combined with (4), equation (7) becomes

$$\boxed{\boldsymbol{\nabla}\phi^{p}.\boldsymbol{n} = \left(\frac{\partial\boldsymbol{\xi}}{\partial t} - \boldsymbol{u}^{\infty}\right).\boldsymbol{n} \quad \text{on } \Sigma_{(t)}.} \tag{9}$$

Finally, since ϕ^{p} is defined up to a constant, we arbitrarily impose

$$\boxed{\phi^{p} = o(1) \quad \text{on } \partial\Omega^{\infty},} \tag{10}$$

to ensure the uniqueness of the solution. Now that the set of equations describing the potential of perturbations ϕ^{p} have been exhibited (boxed equations in this section), it is necessary to obtain a formulation allowing to find a numerical approximation of the solution of this problem.

2.2. Boundary integral representation

The system describing this problem could be determined using the finite element method, by introducing a variational formulation of the Laplace equation coupled to its boundary condition. However, if the solid is evolving in an infinitely large fluid medium, then a very large volume of fluid will be necessary to avoid any artificial confinement effects (Liu et al, 2009), leading to the manipulation of very large number of degrees of freedom. Instead, the solution presented here is based on the boundary integral equations, enabling to manipulate only fluid degrees of freedom located at the fluid-structure interface: the equations on $\Omega^{f}_{(t)}$ are condensed on $\Sigma_{(t)}$.

The Green function G associated with Laplace equation in three dimensions (Bonnet, 1999) is defined as

$$\begin{aligned} G(\boldsymbol{x},\boldsymbol{y}) &= -\frac{1}{4\pi(\boldsymbol{x}-\boldsymbol{y})} \\ \boldsymbol{\nabla}_{\boldsymbol{x}} G(\boldsymbol{x}-\boldsymbol{y}) &= \frac{\boldsymbol{x}-\boldsymbol{y}}{4\pi\left\|\boldsymbol{x}-\boldsymbol{y}\right\|^{2}} \quad \forall \boldsymbol{x},\boldsymbol{y} \in \Omega^{\infty}\times\Omega^{\infty} \\ \Delta_{\boldsymbol{x}} G_{(\boldsymbol{x}-\boldsymbol{y})} &= \delta_{(\boldsymbol{x}-\boldsymbol{y})}, \end{aligned} \tag{11}$$

where δ denotes the dirac distribution. Since $\partial\Omega^\infty \cup \Sigma_{(t)}$ is an enclosing boundary of the fluid volume $\Omega^f_{(t)}$, the Green identity can be applied as

$$\forall \boldsymbol{y} \in \Omega^\infty, \quad \int_{\Omega^f_{(t)}} \Delta_{\boldsymbol{x}} G_{(\boldsymbol{x}-\boldsymbol{y})} \phi^p_{(\boldsymbol{x})} - \Delta\phi^p_{(\boldsymbol{x})} G_{(\boldsymbol{x}-\boldsymbol{y})} \mathrm{d}\Omega_{(\boldsymbol{x})} = \ldots$$
$$\oint_{\Sigma_{(t)}\cup\partial\Omega^\infty} \boldsymbol{\nabla}_{\boldsymbol{x}} G_{(\boldsymbol{x}-\boldsymbol{y})}.\boldsymbol{n}_{(\boldsymbol{x})} \phi^p_{(\boldsymbol{x})} - \boldsymbol{\nabla}\phi^p_{(\boldsymbol{x})}.\boldsymbol{n}_{(\boldsymbol{x})} G_{(\boldsymbol{x}-\boldsymbol{y})} \mathrm{d}\Sigma_{(\boldsymbol{x})} \tag{12}$$

The boundary conditions (6) and (10) combined with the properties

$$\begin{aligned} G_{(\boldsymbol{x}-\boldsymbol{y})} &= o\left(\frac{1}{r}\right) \quad \forall \boldsymbol{x} \in \partial\Omega^\infty \\ \boldsymbol{\nabla}_{\boldsymbol{x}} G_{(\boldsymbol{x}-\boldsymbol{y})} &= o\left(\frac{1}{r^2}\right) \quad \forall \boldsymbol{x} \in \partial\Omega^\infty, \end{aligned} \tag{13}$$

enable to neglect the integral on the border $\partial\Omega^\infty$. The property (Veron, 2016)

$$\int_{\Omega^f_{(t)}} \Delta_{\boldsymbol{x}} G_{(\boldsymbol{x}-\boldsymbol{y})} \phi^p_{(\boldsymbol{x})} \mathrm{d}\Omega = \ldots$$
$$\phi^p_{(\boldsymbol{y})} \left(1 + \oint_{\Sigma_{(t)}} \boldsymbol{\nabla}_{\boldsymbol{x}} G_{(x-y)}.\boldsymbol{n}_{(x)} \mathrm{d}\Sigma_{(x)}\right) \quad \forall \boldsymbol{y} \in \Omega^\infty, \tag{14}$$

combined with equations (5) and (12), gives

$$\boxed{\begin{aligned} \phi^p_{(y)} = &\int_{\Sigma_{(t)}} \boldsymbol{\nabla}_{\boldsymbol{x}} G_{(\boldsymbol{x}-\boldsymbol{y})}.\boldsymbol{n}_{(\boldsymbol{x})} \left(\phi^p_{(\boldsymbol{x})} - \phi^p_{(\boldsymbol{y})}\right) \\ &+ G_{(\boldsymbol{x}-\boldsymbol{y})} \left(\boldsymbol{u}^\infty_{(\boldsymbol{x})} - \frac{\partial \boldsymbol{\xi}_{(\boldsymbol{x})}}{\partial t}\right).\boldsymbol{n}_{(\boldsymbol{x})} \mathrm{d}\Sigma_{(\boldsymbol{x})} \forall \boldsymbol{y} \in \Sigma_{(t)}. \end{aligned}} \tag{15}$$

2.3. Linearized formulation on a reference interface

2.3.1. *Reference configuration*

The linearized equations will be derived relatively to a reference position $\overline{\Sigma}$, arbitrarily set to be the fluid-structure interface in the absence of deformations: $\Sigma_{(\boldsymbol{\xi}=\boldsymbol{0})}$. This will allow to express the physical variables evolving on the time dependant interface $\Sigma_{(t)}$ as a function of the reference space $\overline{\Sigma}$, as detailed in (Pfister, 2019). The functions defined on $\overline{\Sigma}$ are written

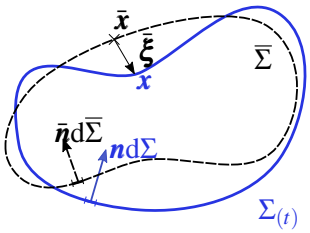

Figure 2. Reference and physical domains.

with a bar $\overline{(.)}$ and we can therefore define the position of the physical interface $\boldsymbol{x} \in \Sigma_{(t)}$ as

$$\bar{\boldsymbol{\xi}}_{(\bar{\boldsymbol{x}},t)} = \boldsymbol{x}_{(\bar{\boldsymbol{x}},t)} - \bar{\boldsymbol{x}} \quad \forall \bar{\boldsymbol{x}} \in \overline{\Sigma}, \tag{16}$$

which is the common definition of the displacement in solid mechanics written in a Lagrangian formalism (hence inherent to a moving material point). Similarly, one can express an oriented infinitesimal element of surface $\boldsymbol{n}\mathrm{d}\Sigma$ (see Figure 2) with Nanson's formula (Holmes, 2009):

$$\boldsymbol{n}_{(\boldsymbol{x})}\mathrm{d}\Sigma_{(\boldsymbol{x})} = \det\left(\bar{\mathbb{F}}_{(\bar{\boldsymbol{\xi}})}\right) \bar{\mathbb{F}}^{-T}_{(\bar{\boldsymbol{\xi}})} \bar{\boldsymbol{n}}_{(\bar{\boldsymbol{x}})} \mathrm{d}\overline{\Sigma}_{(\bar{\boldsymbol{x}})} \quad \forall \bar{\boldsymbol{x}} \in \overline{\Sigma}, \tag{17}$$

where $\bar{\boldsymbol{n}}\mathrm{d}\overline{\Sigma}$ denotes the unit normal times an infinitesimal area on the reference surface $\overline{\Sigma}$ (which is therefore different from the time dependant one). Superscript $(.)^{-T}$ denotes the inverse of a transposed tensor, and $\bar{\mathbb{F}}$ is the deformation gradient defined as

$$\bar{\mathbb{F}}_{(\bar{\boldsymbol{\xi}})} = \left(\mathbb{1} + \overline{\underline{\nabla}}\bar{\boldsymbol{\xi}}\right). \tag{18}$$

We also define the fluid flow with respect to the reference interface

$$\bar{\phi}^p_{(\bar{\boldsymbol{x}})} \equiv \phi^p_{(\boldsymbol{x})}, \quad \bar{\boldsymbol{u}}^p_{(\bar{\boldsymbol{x}})} \equiv \boldsymbol{u}^p_{(\boldsymbol{x})} \quad \forall \bar{\boldsymbol{x}} \in \overline{\Sigma} \tag{19}$$

where $\equiv$ stands for "is defined as", as well as the Green function and its normal derivative

$$\begin{aligned} \overline{\boldsymbol{G}_{\boldsymbol{n}}}_{(\bar{\boldsymbol{x}},\bar{\boldsymbol{y}})}\mathrm{d}\overline{\Sigma}_{(\bar{\boldsymbol{x}})} &\equiv G_{(\boldsymbol{x}-\boldsymbol{y})}\boldsymbol{n}_{(x)}\mathrm{d}\Sigma_{(x)} && \forall \bar{\boldsymbol{x}}, \bar{\boldsymbol{y}} \in \overline{\Sigma} \\ \overline{\partial_n G}_{(\bar{\boldsymbol{x}},\bar{\boldsymbol{y}})}\mathrm{d}\overline{\Sigma}_{(\bar{\boldsymbol{x}})} &\equiv \boldsymbol{\nabla}_x G_{(\boldsymbol{x}-\boldsymbol{y})}.\boldsymbol{n}_{(\boldsymbol{x})}\mathrm{d}\Sigma_{(\boldsymbol{x})} && \forall \bar{\boldsymbol{x}}, \bar{\boldsymbol{y}} \in \overline{\Sigma}. \end{aligned} \tag{20}$$

It is important to notice that equations (16), (19) and (20) differ from (17): the first ones define an equality between the parameters on the physical and reference spaces whereas $\boldsymbol{n}\mathrm{d}\Sigma$ undergoes a transformation relatively to the reference configuration $\bar{\boldsymbol{n}}\mathrm{d}\overline{\Sigma}$. The way

$\bar{\phi}^p$ is defined isn't inherent to a moving fluid particle contrarily to a Lagrangian definition, but results from their observation on a point moving in space which also differs from the Eulerian definition that observes particles properties on a fixed point of space: this is the reason why this method might be referred to as an Arbitrary Lagrangian Eulerian (ALE) approach (Pfister, 2019). The ambient flow parametrized with respect to the reference position is defined as:

$$\bar{\boldsymbol{u}}^{\infty}_{(\bar{\boldsymbol{x}})} = \boldsymbol{u}^{\infty}_{(\boldsymbol{x})} \quad \forall \bar{\boldsymbol{x}} \in \overline{\Sigma}. \tag{21}$$

By combining (9), (16), (17), (19) and (21) we deduce

$$G_{(\boldsymbol{x}-\boldsymbol{y})} \boldsymbol{\nabla} \phi^p_{(\boldsymbol{x})} . \boldsymbol{n}_{(\boldsymbol{x})} \mathrm{d}\Sigma_{(\boldsymbol{x})} = \overline{\boldsymbol{G_n}}_{(\bar{\boldsymbol{x}}-\bar{\boldsymbol{y}})} \cdot \left(\frac{\partial \bar{\boldsymbol{\xi}}}{\partial t}_{(\bar{\boldsymbol{x}})} - \bar{\boldsymbol{u}}^{\infty}_{(\bar{\boldsymbol{x}})} \right) \mathrm{d}\overline{\Sigma} \quad \forall \bar{\boldsymbol{x}}, \bar{\boldsymbol{y}} \in \overline{\Sigma}. \tag{22}$$

The integral representation written on the reference configuration is then given by:

$$\boxed{\bar{\phi}^p_{(\bar{\boldsymbol{y}})} = \int_{\overline{\Sigma}} \overline{\partial_n G}_{(\bar{\boldsymbol{x}}-\bar{\boldsymbol{y}})} \left(\bar{\phi}^p_{(\bar{\boldsymbol{x}})} - \bar{\phi}^p_{(\bar{\boldsymbol{y}})} \right) + \overline{\boldsymbol{G_n}}_{(\bar{\boldsymbol{x}}-\bar{\boldsymbol{y}})} \cdot \left(\bar{\boldsymbol{u}}^{\infty}_{(\bar{\boldsymbol{x}})} - \frac{\partial \bar{\boldsymbol{\xi}}}{\partial t}_{(\bar{\boldsymbol{x}})} \right) \mathrm{d}\overline{\Sigma} \quad \forall \bar{\boldsymbol{y}} \in \overline{\Sigma}} \tag{23}$$

2.3.2. *Linearized equations*

This section will introduce a linearized formulation of the integral representation (23), made possible thanks to the small perturbations hypothesis :

$$\begin{aligned} \mathscr{D} = \frac{\|\boldsymbol{\xi}\|}{L} \ll 1 \\ \left\| \underline{\underline{\nabla}} \boldsymbol{\xi} \right\| \ll 1, \end{aligned} \tag{24}$$

which allows to decompose the interface position, by denoting with a superscript $(.)^1$ the variables with a negligible amplitude relatively to those denoted with a superscript $(.)^0$:

$$\bar{\boldsymbol{\xi}}^{\,1}(\bar{\boldsymbol{x}}^0) = \boldsymbol{x} - \bar{\boldsymbol{x}}^0 \quad \forall \bar{\boldsymbol{x}}^0 \in \overline{\Sigma}, \tag{25}$$

resulting from $\mathscr{D} \ll 1$. In the following equations, the superscript $(.)^1$ will not only attach informations on the first order amplitude of a variable, but will as well define its linearity to the displacements $\bar{\boldsymbol{\xi}}^{\,1}$ (this linearity being obvious for $\bar{\boldsymbol{\xi}}^{\,1}$ itself). Because of the small perturbations hypothesis (24), it is possible to linearize Nanson's formula (17) (*h.o.t* is for higher order terms):

$$\boldsymbol{n} \mathrm{d}\Sigma_{(t)} = (\boldsymbol{n}^0 + \boldsymbol{n}^1) \mathrm{d}\overline{\Sigma} + h.o.t \quad \text{on } \overline{\Sigma}, \tag{26}$$

and the Green function (20), similarly to the method presented by (Potthast, 1994) for acoustic applications:

$$\begin{aligned} \overline{\boldsymbol{G_n}} &= \overline{\boldsymbol{G_n}}^0 + \overline{\boldsymbol{G_n}}^1 + h.o.t \qquad \text{on } \overline{\Sigma} \\ \overline{\partial_n G} &= \overline{\partial_n G}^0 + \overline{\partial_n G}^1 + h.o.t \qquad \text{on } \overline{\Sigma}. \end{aligned} \tag{27}$$

Detailed expressions of (26) and (27) can be found in appendix 6. The strain rate of an irrotational ambient flow is:

$$\mathbb{D}^{\infty} = \frac{1}{2} \left(\underline{\underline{\nabla}} \boldsymbol{u}^{\infty} + \underline{\underline{\nabla}}^T \boldsymbol{u}^{\infty} \right). \tag{28}$$

If the convection of the ambient flow by the interface displacements is small, hence for

$$\left\| \mathbb{D}^{\infty} \boldsymbol{\xi}^{\,1} \right\| = o\left(U^{\infty}\right), \tag{29}$$

the velocity at order zero and one at the interface is obtained with a Taylor series (Galper, 1995):

$$\begin{aligned} \boldsymbol{u}^{\infty}_{(\boldsymbol{x})} &= \boldsymbol{u}^{\infty}_{(\bar{\boldsymbol{x}})} + \mathbb{D}^{\infty} \boldsymbol{\xi}^{\,1} + h.o.t. \\ \bar{\boldsymbol{u}}^{\infty 0}_{(\bar{\boldsymbol{x}})} &= \boldsymbol{u}^{\infty}_{(\bar{\boldsymbol{x}})} \\ \bar{\boldsymbol{u}}^{\infty 1}_{(\bar{\boldsymbol{x}})} &= \mathbb{D}^{\infty} \bar{\boldsymbol{\xi}}^{\,1}_{(\bar{\boldsymbol{x}})} = o\left(U^{\infty}\right). \end{aligned} \tag{30}$$

Under the assumption that the structure velocity is small relatively to the ambient flow, the normal velocity of the structure is given by:

$$\frac{\partial \boldsymbol{\xi}}{\partial t} = \frac{\partial \bar{\boldsymbol{\xi}}^{\,1}}{\partial t} = o\left(U^{\infty}\right) \tag{31}$$

Based on equations (23), (25), (27), (30) and (31), a linearization of the potential $\bar{\phi}^p$ is introduced such that

$$\begin{aligned} \bar{\phi}^p_{(\bar{\boldsymbol{x}})} &\equiv \phi^p_{(\boldsymbol{x})} \qquad \text{on } \overline{\Sigma}, \\ \bar{\phi}^p_{(\bar{\boldsymbol{x}})} &= \bar{\phi}^{p0}_{(\bar{\boldsymbol{x}})} + \bar{\phi}^{p1}_{(\bar{\boldsymbol{x}})} + h.o.t \qquad \text{on } \overline{\Sigma}. \end{aligned} \tag{32}$$

We can therefore obtain the linearization of the integral representation (23)

$$\begin{aligned}
\bar{\phi}^{p0}_{(\bar{\mathbf{y}})} &= \int_{\overline{\Sigma}} \overline{\partial_n G}^{0}_{(\bar{\mathbf{x}}-\bar{\mathbf{y}})} \left(\bar{\phi}^{p0}_{(\bar{\mathbf{x}})} - \bar{\phi}^{p0}_{(\bar{\mathbf{y}})}\right) \\
&\quad + \overline{\boldsymbol{G}_{\boldsymbol{n}}}^{0}_{(\bar{\mathbf{x}}-\bar{\mathbf{y}})} . \bar{\boldsymbol{u}}^{\infty}_{(\bar{\mathbf{x}})} \mathrm{d}\overline{\Sigma} \qquad \forall \bar{\mathbf{y}} \in \overline{\Sigma} \\
\bar{\phi}^{p1}_{(\bar{\mathbf{y}})} &= \int_{\overline{\Sigma}} \overline{\partial_n G}^{0}_{(\bar{\mathbf{x}}-\bar{\mathbf{y}})} \left(\bar{\phi}^{p1}_{(\bar{\mathbf{x}})} - \bar{\phi}^{p1}_{(\bar{\mathbf{y}})}\right) \\
&\quad + \overline{\partial_n G}^{1}_{(\bar{\mathbf{x}}-\bar{\mathbf{y}})} \left(\bar{\phi}^{p0}_{(\bar{\mathbf{x}})} - \bar{\phi}^{p0}_{(\bar{\mathbf{y}})}\right) \\
&\quad + \overline{\boldsymbol{G}_{\boldsymbol{n}}}^{0}_{(\bar{\mathbf{x}}-\bar{\mathbf{y}})} . \left(\mathbb{D}^{\infty} \boldsymbol{\xi}^{1} - \frac{\partial \boldsymbol{\xi}^{1}}{\partial t}\right) \\
&\quad + \overline{\boldsymbol{G}_{\boldsymbol{n}}}^{1}_{(\bar{\mathbf{x}}-\bar{\mathbf{y}})} . \bar{\boldsymbol{u}}^{\infty 0}_{(\bar{\mathbf{x}})} \mathrm{d}\overline{\Sigma} \qquad \forall \bar{\mathbf{y}} \in \overline{\Sigma}.
\end{aligned} \tag{33}$$

The above equations allow to calculate ϕ^p by using variables only on the reference configuration. The differentiability of BEM operators had already been studied in the fields of acoustics (Potthast, 1994). However, to the knowledge of the authors, the application of this kind of method to flowing incompressible flow has not been exhibited in the literature . In order to obtain the whole linearized velocity potential ϕ, we need to introduce the linearized variations of the ambient potential ϕ^{∞} using a Taylor expansion at the first order, which is valid since ϕ^{∞} is defined on the whole Ω^{∞} domain:

$$\begin{aligned}
\bar{\phi}^{\infty}_{(\bar{\mathbf{x}})} &\equiv \phi^{\infty}_{(\boldsymbol{x})} && \forall \bar{\boldsymbol{x}} \quad \text{on } \overline{\Sigma}, \\
\bar{\phi}^{\infty 0}_{(\bar{\mathbf{x}})} &= \phi^{\infty}_{(\boldsymbol{x}^0)} && \forall \bar{\boldsymbol{x}} \quad \text{on } \overline{\Sigma}, \\
\bar{\phi}^{\infty 1}_{(\bar{\mathbf{x}})} &= \boldsymbol{\nabla} \phi^{\infty}_{(\boldsymbol{x}^0)} . \boldsymbol{\xi}^{1} = \boldsymbol{u}^{\infty}_{(\boldsymbol{x}^0)} . \boldsymbol{\xi}^{1} && \forall \bar{\boldsymbol{x}} \quad \text{on } \overline{\Sigma}.
\end{aligned} \tag{34}$$

The linear potential of the ambient flow perturbed by the vibrating solid can therefore be expressed as

$$\phi = \bar{\phi}^{p0} + \bar{\phi}^{p1} + \bar{\phi}^{\infty 0} + \bar{\phi}^{\infty 1} + h.o.t \quad \text{on } \Sigma_{(t)}. \tag{35}$$

The velocity $\boldsymbol{u}$ at orders zero and one can be calculated using the gradient and the potential from the reference configuration (Pfister, 2019):

$$\bar{\boldsymbol{u}}^{0} = \overline{\boldsymbol{\nabla}} \bar{\phi}^{0}, \quad \bar{\boldsymbol{u}}^{1} = \overline{\boldsymbol{\nabla}} \bar{\phi}^{1} - \overline{\underline{\nabla}}^{T} \bar{\boldsymbol{\xi}}^{1} \bar{\boldsymbol{u}}^{0} \quad \text{on } \overline{\Sigma}. \tag{36}$$

The equations exhibited are valid based on hypothesis that will be discussed in the following section, with a particular attention to the case of airships.

2.4. Hypothesis of the model

The wall boundary condition is valid if the fluid can be considered as inviscid, hence when hypotheses (8) are met. Regarding airships, this seems to be valid to a certain extent: airships evolve at high Reynolds numbers because of their large dimensions. However, (Lutz et al, 2002) showed that the hull alone can produce lift even at small angles of attack, which means a correction for taking into account circulation effects on the fluid might be necessary to take into account a wider range of effects. However, for large angles of attack separation appears, which isn't predictable by this model which supposes turbulence is negligible and the flow is attached. The small perturbations of the solid (30) and (31) are reasonable approximations regarding the deformation of the hull's membrane if the steady deformed configuration is considered as the reference interface: taking the stress free configuration as a reference isn't a reasonable approach, since the deformations between the stress free and steady deformed configurations are expected to be large, requiring to take into account geometric non linearities. However, regarding the rigid body motions, the small displacements hypothesis is a limitation: in order to expand the model to any flight configuration, an extension to large displacements coupled with small deformation would be of high interest, inspired from the works of (Thomasson et al, 2013) dealing with rigid body motions in currents for example. Furthermore, the lack of orders higher than 1 to describe the potential is compensated by the ability to predict how instabilities might grow exponentially from small perturbations, which is of high interest in aerodynamics (Theodorsen, 1949; Dowell, 1989).

3. BOUNDARY ELEMENT METHOD IMPLEMENTATION

3.1. Numerical procedure

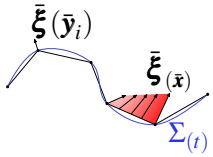

Figure 3. BEM mesh of $\Sigma_{(t)}$, with collocation point $\bar{\mathbf{y}}_i$ on each node and a linear interpolation of $\bar{\boldsymbol{\xi}}_{(\bar{\mathbf{x}})}$ on each element.

In order to find a numerical approximation to the solution associated with equation (33) for a steady ambient flow, we introduce the BEM method which

approximates the integral over the fluid-structure interface (Bonnet, 1999). The interface is discretised into n_e elements and n nodes, where the variables are interpolated using linear basis functions attached to the mesh nodes. According to the collocation method, the evaluation points $\boldsymbol{y}_i$ are also located on the mesh nodes, see figure 3. We introduce the operators $[S]_{n\times 3n}$, $[S']_{n\times 3n}$ (single layer operators) and $[D]_{n\times n}$, $[D']_{n\times 3n}$ (double layer operators), defined as follows:

$$
\begin{aligned}
\sum_j [S]_{ij} \{\bar{\boldsymbol{u}}\}_j &\simeq \int_{\bar{\Sigma}} \overline{\boldsymbol{G}}^0_{(\boldsymbol{x},\boldsymbol{y}_i)} \cdot \bar{\boldsymbol{u}}_{(\bar{\boldsymbol{x}})} \mathrm{d}\bar{\Sigma}_{(\bar{\boldsymbol{x}})} \\
\sum_j \left[S'_{(\bar{\boldsymbol{u}}^\infty)}\right]_{ij} \left\{\bar{\boldsymbol{\xi}}\right\}_j &\simeq \int_{\bar{\Sigma}} \overline{\boldsymbol{G}}^1_{(\boldsymbol{x},\boldsymbol{y}_i,\bar{\boldsymbol{\xi}})} \cdot \bar{\boldsymbol{u}}^{\infty 0}_{(\bar{\boldsymbol{x}})} \mathrm{d}\bar{\Sigma}_{(\bar{\boldsymbol{x}})} \\
\sum_i [D]_{ij} \{\bar{\phi}\}_j &\simeq \int_{\bar{\Sigma}} \overline{\partial_n G}^0_{(\boldsymbol{x},\boldsymbol{y}_i)} \bar{\phi} \mathrm{d}\bar{\Sigma}_{(\bar{\boldsymbol{x}})} \\
\sum_i \left[D'_{(\bar{\phi})}\right]_{ij} \left\{\bar{\boldsymbol{\xi}}\right\}_j &\simeq \int_{\bar{\Sigma}} \overline{\partial_n G}^1_{(\boldsymbol{x},\boldsymbol{y}_i,\bar{\boldsymbol{\xi}})} \left(\bar{\phi}_{(\bar{\boldsymbol{x}})} - \bar{\phi}_{(\bar{\boldsymbol{y}})}\right) \mathrm{d}\bar{\Sigma}_{(\bar{\boldsymbol{x}})},
\end{aligned}
\tag{37}
$$

where the brackets $[.]$ denote matrices and $\{.\}$ denotes a $n-$sized vector, its i^{th} component being the value of the variable at the node $\bar{\boldsymbol{y}} = \bar{\boldsymbol{y}}_i$. Because of the linearization, BEM operators are only calculated once, allowing to take into account variations associated to any small mesh deformation without recalculating the discretized operators for the BEM as done in previous studies on fluid structure interaction (Veron et al, 2016; Riccardi et al, 2020), at the price of stocking four matrix operators instead of two. The zero and first order solutions of the potential can be obtained by inverting the linear systems with a GMRes algorithm:

$$
\begin{aligned}
([I_d] - [D]) \left\{\phi^{p0}\right\} &= [S] \left\{\bar{\boldsymbol{u}}^{\infty 0}\right\} \\
([I_d] - [D]) \left\{\phi^{p1}\right\} &= \left(\left[D'_{(\bar{\phi}^{p0})}\right] + \left[S'_{(\bar{\boldsymbol{u}}^\infty)}\right]\right) \left\{\bar{\boldsymbol{\xi}}^1\right\} \\
&\quad + [S] \left(\left\{\bar{\boldsymbol{u}}^{\infty 1}\right\} - \left\{\frac{\partial \bar{\boldsymbol{\xi}}^1}{\partial t}\right\}\right)
\end{aligned}
\tag{38}
$$

Because the expression of $\left[D'_{(\bar{\phi}^{p0})}\right]$ depends on the field $\bar{\phi}^{p0}$, this operator has to be computed once the zero order system has been solved.

3.2. Validation

Equation (38) shows that the first order solution of the velocity potential ϕ^p is composed of two parts, proportional respectively to the position $\bar{\boldsymbol{\xi}}$ and the velocity $\frac{\partial \bar{\boldsymbol{\xi}}}{\partial t}$ of the structure, and referred as the quasi-steady and the vibration components. In order to ensure that the solution associated with each of these contributions is well predicted by the theory and the numerical computation, two test cases are presented.

3.2.1. *Vibration component*

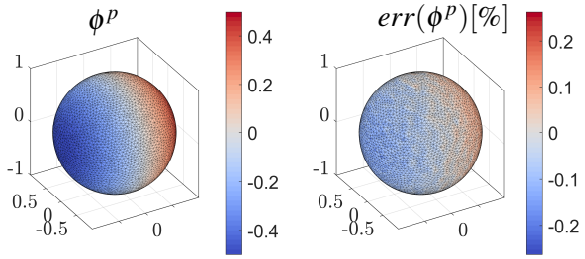

Figure 4. Velocity potential induced by a sphere oscillating in a fluid at rest.

When the structure vibrates, its normal velocity is transmitted to the fluid via the fluid-structure interface, which is responsible for the added mass effect amongst others. The numerical results provided by the BEM associated to vibrations $\frac{\partial \bar{\boldsymbol{\xi}}}{\partial t}$, for $\bar{\boldsymbol{\xi}} = 0$, are compared to analytical results in the case of a sphere in a resting fluid (Veron, 2016). The results presented in figure 4 show a maximal relative error of 0.2% when compared with theoretical results. One can notice that the solution at order 0 is solved by inverting the same linear system with the imposed boundary velocity $\frac{\partial \bar{\boldsymbol{\xi}}}{\partial t}$ being replaced by $-\bar{\boldsymbol{u}}^{\infty 0}$,which means the potential ϕ^{p0} can be approximated numerically with a similar accuracy.

3.2.2. *Quasi steady component*

The term proportional to the displacement $\bar{\boldsymbol{\xi}}$ in equation (38) is referred as "quasi static" because it is the solution found when the deformations occur at a negligible velocity. In order to verify if the linearization of the quasi steady potential is valid or not, the results of the first order solution $\bar{\phi}^{p1}$ associated with a steady homogeneous ambient flow are compared with the variation of the zero order solution ϕ^{p0} obtained by actually deforming the mesh, hence calculating new BEM operators $[S]$ and $[D]$ on consecutive mesh positions.

Figure 5 compares the variation of the potential as predicted by the linearization (for $\frac{\partial \bar{\boldsymbol{\xi}}}{\partial t} = 0$) (top half),

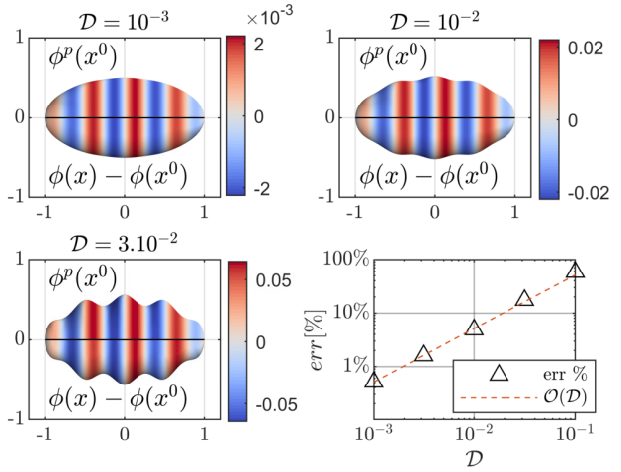

Figure 5. Permanent flow potential variations around a deformed ellipsoid. The top half of each figure is the linear prediction $\bar{\phi}^{p1}$ from the initial mesh, and the bottom half is the potential variation calculated with finite differences between the original and deformed mesh. The shape of deformation is the same in each graph, and the amplitude of deformation is represented at real scale. Bottom right graph shows the evolution of the maximal error on the linear prediction ϕ^p as a function of $\mathscr{D}$.

whereas the bottom half was obtained by deforming the mesh and applying finite differences on an degenerated sphere mesh of ≈ 7000 nodes, with semi axis of 1 and 0.5. The side view was chosen because of the axisymmetry of the problem. The error is defined as

$$err = \frac{\max\left(\phi^0_{(x^0)} + \phi^p_{(x^0,\xi^1)} - \phi_{(x)}\right)}{\max\left(\phi^0_{(x^0)} - \phi_{(x)}\right)}. \qquad (39)$$

The bottom right graph shows that the maximal error of the linear prediction is linear to the displacement number for small perturbations up to $\mathscr{D} < 10^{-2}$. For higher values of $\mathscr{D}$, the error becomes higher than the linear trend at small displacement number. However, looking at the bottom left of figure 5, the geometry associated with $\mathscr{D} > 3.10^{-2}$ shows important deformations which are out of the scope of this linear model. The shape of the deformation presented here shows good agreement (less than 1% error) with the linear prediction of the potential ϕ until $\mathscr{D} < 2.10^{-}3$, however for deformations with a more regular shape (hence with less lobes on the surface for example) the prediction would be more accurate according to the small gradient hypothesis (24).

4. CONCLUSION

4.1. Summary and main results

A new method to solve linearized potential of the fluid induced by a structure undergoing small deformations over time is introduced. The linear version of the equations only requires to calculate two additional operators on the reference mesh in order to obtain an approximated solution when the fluid-structure interface undergoes deformations, reducing drastically the calculation costs with respect to the computation of new BEM operators at each deformation.

4.2. Work in progress and perspectives

The pressure resulting from the potential solution is currently being determined analytically from (Nitikitpaiboom, 1993), and its implementation will allow to determine the fluid induced loads on the airship's hull. The linearized formulation will allow as well to put forward added mass, damping and stiffness by the fluid on the hull, as explained by the authors in (Schotté et al, 2019), allowing to determine possible instabilities of the airship induced by the coupling with a heavy fluid. As mentioned in section 3.2.2, an important part of the work will consist in comparing non linear and linear approaches on test cases to determine the validity of the approach depending on the problem solved. Another perspective is the coupling of the small strains of the structure with large rigid body displacements, or with circulation contributions.

5. REFERENCES

G. Riccardi and E. De Bernardis, 2019, *Numerical simulations of the dynamics and the acoustics of an axisymmetric bubble rising in an inviscid liquid, European Journal of Mechanics - B/Fluids, vol. 79, p. 121-140.*

Pfister, J.-L., Instabilities and optimization of elastic structures interacting with laminar flows, Doctoral dissertation, Paris.

Liu, J. et al, 2010, *Numerical Investigation on the Aeroelastic Behavior of an Airship with Hull-Fin Configuration. J Hydrodyn 22, 207-213.*

Galper, A. and T. Miloh, 1995, Dynamic equations of motion for a rigid or deformable body in an ar-

bitrary non-uniform potential flow field, Journal of Fluid Mechanics 295, 91–120.

Veron, E. and Bouzidi, R., 2016, *Large displacements of light thin flexible structures coupled with heavy fluids using co-simulation between finite element and fast boundary element solvers, FIV 2016.*

Veron, E., 2016, Calcul numérique des grandes dformations de structures minces en contact avec des fluides lourds. Doctoral dissertation, Nantes.

Nitikitpaiboon, C. and Bathe, K.-J., 1993, *An arbitrary lagrangian-eulerian velocity potential formulation for fluid-structure interaction Computers and Structures, 47, pp. 871-891.*

Li, Y. et al, 2009. Dynamics Modeling and Simulation of Flexible Airships. AIAA Journal 47, 592-605.

Bonnet, M., 1999, *Boundary integral equation methods for solids and fluids. Wiley.*

Holmes, M. H., 2009, Introduction to the foundations of applied mathematics.

Theodorsen, T., 1949, *General theory of aerodynamic instability and the mechanism of flutter., NACA Technical Report 496.*

Dowell, E. H., 1989, A modern course in aeroelasticity Eds. Howard C. Curtiss, Robert H. Scanlan, and Fernando Sisto. Vol. 3. Dordrecht, The Netherlands: Kluwer academic publishers.

Potthast, R., 1994,, *Fréchet differentiability of boundary integral operators in inverse acoustic scattering. Inverse Problems, 10(2), 431.*

Schotté, J.S., Doaré, O., Le Mestre, R., 2019, Effect of coupling with internal and external fluids on the mechanical behaviour of aerostats, SEMC 2019.

Lutz, T. et al, 2002, *Summary of Aerodynamic Studies on the Lotte Airship 4th International Airship Convention and Exhibition, Cambridge, England.*

Thomasson, P. G. and Woolsey, C. A., 2013, Vehicle motion in currents, IEEE journal of oceanic engineering, vol. 38.

6. APPENDIX A: DETAILED CALCULATION OF THE LINEARISATION

We detail here how the linearisation was performed. Under the small displacement assumption, the values of the oriented surface is given by (Holmes, 2009)

$$\begin{aligned}\boldsymbol{n}^0 \mathrm{d}\overline{\Sigma} &= \bar{\boldsymbol{n}} \mathrm{d}\overline{\Sigma} \\ \boldsymbol{n}^1 \mathrm{d}\overline{\Sigma} &= \left(\underline{\underline{\bar{\nabla}}}.\boldsymbol{\xi}^1 - \underline{\underline{\bar{\nabla}}}^T \boldsymbol{\xi}^1 \right) \bar{\boldsymbol{n}} \mathrm{d}\overline{\Sigma}.\end{aligned} \tag{40}$$

The surface gradients are defined on the reference surface for any scalar $\bar{a}$ and vector $\bar{\boldsymbol{b}}$ on $\overline{\Sigma}$:

$$\begin{aligned}\bar{\boldsymbol{\nabla}}_S \bar{a} &\equiv \bar{\boldsymbol{\nabla}} \bar{a} - (\bar{\boldsymbol{\nabla}} \bar{a}.\bar{\boldsymbol{n}})\bar{\boldsymbol{n}} && \text{on } \overline{\Sigma} \\ \underline{\underline{\bar{\nabla}}}_S^T \bar{\boldsymbol{b}} &\equiv \left(\bar{\boldsymbol{\nabla}}_S(\bar{\boldsymbol{b}}.\boldsymbol{e}_x), \bar{\boldsymbol{\nabla}}_S(\bar{\boldsymbol{b}}.\boldsymbol{e}_y), \bar{\boldsymbol{\nabla}}_S(\bar{\boldsymbol{b}}.\boldsymbol{e}_z) \right) && \text{on } \overline{\Sigma},\end{aligned} \tag{41}$$

one can show that the small variations of $\boldsymbol{n}\mathrm{d}\Sigma_{(t)}$, with $\mathrm{tr}\,()$ denoting the trace operator, equals to:

$$\begin{aligned}\boldsymbol{n}^0 \mathrm{d}\overline{\Sigma} &= \bar{\boldsymbol{n}} \mathrm{d}\overline{\Sigma} \\ \boldsymbol{n}^1 \mathrm{d}\overline{\Sigma} &= \left(\mathrm{tr}\left(\underline{\underline{\bar{\nabla}}}_S^T \boldsymbol{\xi}^1 \right) - \underline{\underline{\bar{\nabla}}}_S^T \boldsymbol{\xi}^1 \right) \bar{\boldsymbol{n}}.\end{aligned} \tag{42}$$

The first order Taylor expansion of the norm of a vector at an arbitrary power n is:

$$\begin{aligned}\|\boldsymbol{x}-\boldsymbol{y}\|^n = &\left\|\boldsymbol{x}^0-\boldsymbol{y}^0\right\|^n \\ &+ n(\boldsymbol{x}^0-\boldsymbol{y}^0).\left(\boldsymbol{\xi}^1(\boldsymbol{x}^0)-\boldsymbol{\xi}^1(\boldsymbol{y}^0)\right)\left\|\boldsymbol{x}^0-\boldsymbol{y}^0\right\|^{n-2} \\ &+ o\left(\boldsymbol{\xi}^1\right).\end{aligned} \tag{43}$$

The Green function given by (11) and its gradient become when combined with the linearized expression (43):

$$\begin{aligned}\overline{\boldsymbol{G}_{\boldsymbol{n}}}^0 &= -\frac{1}{4\pi}\frac{\boldsymbol{n}^0}{\|\boldsymbol{x}^0-\boldsymbol{y}^0\|} \\ \overline{\boldsymbol{G}_{\boldsymbol{n}}}^1 &= \frac{1}{4\pi}\left(\frac{(\boldsymbol{x}^0-\boldsymbol{y}^0).\left(\boldsymbol{\xi}^1{}_{(\boldsymbol{x}^0)}-\boldsymbol{\xi}^1{}_{(\boldsymbol{y}^0)}\right)\boldsymbol{n}^0}{\|\boldsymbol{x}^0-\boldsymbol{y}^0\|^3} - \frac{\boldsymbol{n}^1}{\|\boldsymbol{x}^0-\boldsymbol{y}^0\|}\right) \\ \overline{\partial_n G}^0 &= \frac{1}{4\pi}\frac{(\boldsymbol{x}^0-\boldsymbol{y}^0).\boldsymbol{n}^0}{\|\boldsymbol{x}-\boldsymbol{y}\|^3} \\ \overline{\partial_n G}^1 &= \frac{1}{4\pi}\left(\frac{(\boldsymbol{x}^0-\boldsymbol{y}^0).\boldsymbol{n}^1}{\|\boldsymbol{x}-\boldsymbol{y}\|^3} + \frac{\left(\boldsymbol{\xi}^1{}_{(\boldsymbol{x}^0)}-\boldsymbol{\xi}^1{}_{(\boldsymbol{y}^0)}\right).\boldsymbol{n}^0}{\|\boldsymbol{x}^0-\boldsymbol{y}^0\|^2}\right. \\ &\quad \left. -3\frac{(\boldsymbol{x}^0-\boldsymbol{y}^0).\left(\boldsymbol{\xi}^1{}_{(\boldsymbol{x}^0)}-\boldsymbol{\xi}^1{}_{(\boldsymbol{y}^0)}\right)(\boldsymbol{x}^0-\boldsymbol{y}^0).\boldsymbol{n}^0}{\|\boldsymbol{x}^0-\boldsymbol{y}^0\|^5}\right).\end{aligned} \tag{44}$$